AMERICAN SOCIETY FOR MICROBIOLOGY | Infection and Immunity®

HOST RESPONSE AND INFLAMMATION

Neutrophil-Derived Oncostatin M Triggers Diverse Signaling Pathways during Pneumonia

Katrina E. Traber,[a,b] Ernest L. Dimbo,[a] Anukul T. Shenoy,[a] Elise M. Symer,[a] Eri Allen,[a] Joseph P. Mizgerd,[a,b,c,d] Lee J. Quinton[a,b,c,e]

[a]Pulmonary Center, Boston University School of Medicine, Boston, Massachusetts, USA
[b]Department of Medicine, Boston University School of Medicine, Boston, Massachusetts, USA
[c]Department of Microbiology, Boston University School of Medicine, Boston, Massachusetts, USA
[d]Department of Biochemistry, Boston University School of Medicine, Boston, Massachusetts, USA
[e]Department of Pathology and Laboratory Medicine, Boston University School of Medicine, Boston, Massachusetts, USA

ABSTRACT Pneumonia is a major public health concern, causing significant morbidity and mortality annually despite the broad use of antimicrobial agents. Underlying many of the severe sequelae of acute lung infections is dysfunction of the immune response, which remains incompletely understood yet is an attractive target of adjunct therapy in pneumonia. Here, we investigate the role of oncostatin M (OSM), a pleiotropic cytokine of the interleukin-6 (IL-6) family, and how its signaling modulates multiple innate immune pathways during pneumonia. Previously, we showed that OSM is necessary for neutrophil recruitment to the lungs during pneumonia by stimulating STAT3-driven CXCL5 expression. In this study, transcriptional profiling of whole-lung pneumonia with OSM neutralization revealed 241 differentially expressed genes following only 6 h of infection. Many downregulated genes are associated with STAT1, STAT3, and interferon signaling, suggesting these pathways are induced by OSM early in pneumonia. Interestingly, STAT1 and STAT3 activation was subsequently upregulated with OSM neutralization by 24 h, suggesting that OSM interruption dysregulates these central signaling pathways. When we investigated the source of OSM in pneumonia, neutrophils and, to a lesser extent, macrophages appear to be primary sources, suggesting a positive feedback loop of OSM production by neutrophils. From these studies, we conclude that OSM produced by recruited neutrophils tunes early innate immune signaling pathways, improving pneumonia outcomes.

KEYWORDS oncostatin M, neutrophil, pneumonia

Pneumonia remains a leading cause of death, morbidity, and loss of productive life-years both in the United States and worldwide (1, 2), despite vaccinations, early antibiotics, lung protective ventilatory strategies, and improved supportive care. The causative agents in pneumonia range from bacterial to viral and, occasionally, fungal pathogens (3). Despite differences in microbial pathogenesis, most infections can lead to clinically similar pneumonias, the acute respiratory distress syndrome (ARDS), and sepsis (4). The immune dysfunction underlying pneumonia outcome remains incompletely understood, such that immune-modulating therapies have not yet come to fruition.

Oncostatin M (OSM) is an interleukin-6 (IL-6) family cytokine with established effects on lung fibrosis, malignancy, and acute and chronic inflammation. In human studies, it is upregulated in several acute and chronic inflammatory processes, including but not limited to sepsis (5–7), ARDS (8), allergic rhinitis (9), inflammatory bowel disease (10), and systemic sclerosis (11). Furthermore, OSM is intimately involved in pulmonary inflammatory processes, as elevated OSM is seen in the bronchoalveolar lavage fluid (BALF) of patients with acute lung injury from pneumonia (8). Although there

Citation Traber KE, Dimbo EL, Shenoy AT, Symer EM, Allen E, Mizgerd JP, Quinton LJ. 2021. Neutrophil-derived oncostatin M triggers diverse signaling pathways during pneumonia. Infect Immun 89:e00655-20. https://doi.org/10.1128/IAI.00655-20.

Editor Manuela Raffatellu, University of California San Diego School of Medicine

Copyright © 2021 American Society for Microbiology. All Rights Reserved.

Address correspondence to Katrina E. Traber, katraber@bu.edu.

Received 15 October 2020
Returned for modification 16 November 2020
Accepted 11 January 2021
Accepted manuscript posted online 1 February 2021
Published 17 March 2021

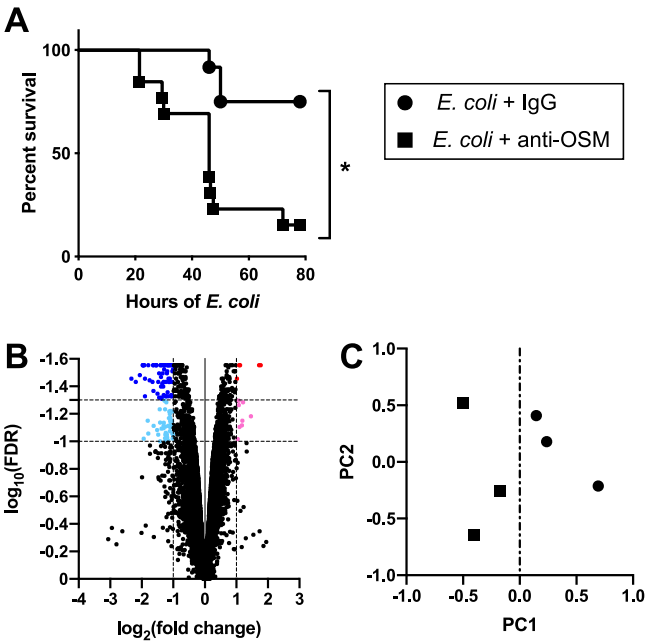

FIG 1 Neutralization of OSM has widespread effects in pneumonia. All experiments were performed over two separate days. Mice were infected with *E. coli* in the presence of anti-OSM or IgG control. (A) Kaplan-Meier survival curve. *, $P < 0.05$ by log-rank (Mantel-Cox) test. IgG, $n = 12$; anti-OSM, $n = 13$. For microarray studies, lungs were harvested after 6 h of *E. coli* pneumonia, $n = 3$ in each group. (B) Volcano plot of $\log_{10}$(FDR) versus $\log_2$(fold change) in control versus anti-OSM-treated mice. Blue and red dots represent genes with a fold change decrease or increase greater than 1, respectively (vertical dashed lines). Darker colors represent genes with FDR of <0.05, and lighter shade indicates FDR of <0.1 (horizontal dashed lines). (C) Principal component analysis (PCA) was performed using all genes (21,187) across all samples (3 control IgG, 3 anti-OSM). The plot shows principal component 1 versus 2, and the dash-dot line represents a PC1 of zero. Each dot is labeled with the respective sample name.

is a strong association between OSM and these processes, the specific effects of OSM during acute pulmonary infections in humans remain unclear and remain a major knowledge gap.

In a murine model of Gram-negative pneumonia, we demonstrated that OSM is induced rapidly after pathogen introduction (12) and is required for maximal neutrophil recruitment (13). OSM exerts this action by inducing the production of the neutrophil chemokine CXCL5 by lung epithelial cells in a STAT3-dependent manner. Although OSM can enhance the recruitment of neutrophils, it appears to do this without significant alterations in bacterial clearance or lung injury, as measured by BALF protein (13). Despite the abundance of data suggesting that OSM plays a central role in pulmonary inflammatory processes, intrapulmonary signals controlled by OSM have not yet been fully elucidated. In the following studies, we sought to identify the biologic pathways that are modulated by the presence or absence of OSM during acute pulmonary infection, along with its cellular sources. Ultimately, it is our hope that by understanding how OSM shapes the immunological environment in the lung during pneumonia, this knowledge could be effectively used to potentiate beneficial outcomes in human pneumonia.

RESULTS

OSM impacts survival and the lung transcriptional landscape during pneumonia. Our prior studies showed that neutralization of OSM during pneumonia leads to a defect in neutrophil recruitment but no changes in lung injury (edema) or bacterial clearance (as measured by colony forming units, CFU, in whole lung or peripheral blood), which left the physiological significance of OSM uncertain (13). To determine whether OSM influenced the outcome of pneumonia, we examined survival in our pneumonia model. Mice with OSM blockade began dying within a day of infection and

nearly all succumbed, whereas most infected mice with intact OSM signaling survived (Fig. 1A). This clear evidence for the physiological significance of OSM signaling in the infected lung prompted us to examine its dynamic effects on pulmonary responses to infection using unbiased approaches.

To determine additional pathways affected by OSM, we investigated transcriptional changes resulting from OSM neutralization during pneumonia. Mice were infected with *Escherichia coli* plus anti-OSM antibody or control IgG for 6 h. RNA was isolated from the involved left lobe, and microarray analysis was performed. Of the 21,187 genes evaluated, neutralization of OSM resulted in 858 differentially expressed genes (DEG; false discovery rate [FDR] of <0.1). Transcripts are represented in a volcano plot (Fig. 1B), where colored dots represent the 125 DEG with a $\log_2$(fold change) greater than 1 or less than -1 and darker shades represent DEG with an FDR of <0.05. These highly significant DEG [FDR < 0.05 and $\log_2$(fold change) > 1 or < -1] are listed in Table 1. Principle component analysis (PCA) was performed across all genes represented on the array, with principal component 1 (PC1) accounting for 40% of the variance in gene expression across the two experimental conditions (Fig. 1C).

We next utilized the Ingenuity Pathway Analysis (IPA) suite for further analysis of our array data. Using the IPA Ingenuity Knowledge Base (14), we determined which of our DEG (FDR < 0.1) were also part of their curated set of genes shown to be affected by OSM. OSM-related DEG are presented in Table 2, and genes that are present in both Table 1 (highly significant DEG) and Table 2 (OSM-related genes) are boldfaced in each table. Of the 48 DEG predicted by IPA to be regulated by OSM, 41 are changed in congruence with prediction (e.g., genes predicted to be upregulated by OSM are decreased with OSM neutralization), with an overall z-score of -5.298 and an overlap *P* value of 7.85×10^{-8}. Among the DEG in our array that are known to be regulated by OSM are cytokines (*Il6*, *Il17a*, and *Csf2*), chemokines (*Ccl2*, *Ccl11*, and *Cxcl10*), interferon-regulated genes (*Irf1*, *Irf7*, *Irf9*, and others), pattern recognition receptors (*Tlr2* and *Tlr3*), and extracellular matrix-modifying proteins (*Adamts4* and *Timp1*). In addition, we have previously shown that OSM induces the production of the chemokine *Cxcl5* (13), which is not on the curated list but is on the list of highly significant DEG. Other DEG not on the IPA list of OSM-associated genes include the chemokine *Cxcl9*, many interferon-regulated genes (*Ifit1*, *Ifit2*, *Ifit3*, and several interferon-responsive genes), and extracellular matrix-modifying proteins (*Ptx3*, *Adamts15*, and *Mmp25*). Finally, among DEG are genes representing functions separate from what was seen in the OSM-associated list, including leukocyte activation markers (*Cd69* and *Cd274/Pdl1*), cytokine receptors (*Il18rap* and *Il2ra*), and the proinflammatory microRNA miR155. Interestingly, many of the DEG are regulated by the same relatively small number of upstream regulators and pathways. Overall, these data show that OSM affects a broad range of early immune responses in lung infections and may do so by modulating upstream regulators.

Using our set of DEG (FDR < 0.1) and the IPA suite, we determined which canonical pathways were associated with OSM neutralization (Fig. 2A). Affected pathways were enriched for innate and adaptive immune pathways (interferon signaling, IL-17 signaling, pattern recognition receptors, and NF-κB signaling), all of which had a neutral or negative z-score, indicating downregulation with neutralization of OSM. We next utilized IPA to determine potential upstream regulators affected by OSM neutralization. We again used DEG (FDR < 0.1) to generate a list of potential upstream regulators (Fig. 2B depicts the top 40 by *P* value of overlap), filtered for genes, RNAs, and proteins. In addition to downregulation of pathways known to be associated with OSM (STAT3 [13] and STAT1 [15]), there was significant downregulation of interferon pathways (alpha, beta, gamma, and lambda interferon as well as IRF3 and IRF7) and other regulators of innate immune responses (NF-κB, tumor necrosis factor alpha, IL-1β, and pathogen recognition receptors). Interestingly, repressors of inflammation (SOCS1, IL10RA, and IL1RN) had divergence of their z-score and gene expression, with a positive z-score and a negative change in gene expression. This suggests that OSM inhibition leads to

TABLE 1 Top downregulated and upregulated DEG[a]

Abbreviation	Name	Log_2(FC)	$-Log_{10}$(FDR)
Ptx3	Pentraxin-related gene	−2.33	1.46
Mx2	Myxovirus (influenza virus) resistance 2	−2.19	1.44
5430427O19Rik	RIKEN cDNA 5430427O19 gene	−2.06	1.48
Ifit3	Interferon-induced protein with tetratricopeptide repeats 3	−1.97	1.56
Csf3	Colony stimulating factor 3 (granulocyte)	−1.96	1.56
Ifit1	Interferon-induced protein with tetratricopeptide repeats 1	−1.96	1.56
Ifit2	Interferon-induced protein with tetratricopeptide repeats 2	−1.93	1.56
Rsad2	Radical *S*-adenosyl methionine domain containing 2	−1.92	1.56
Saa1	Serum amyloid A 1	−1.90	1.46
Gbp5	Guanylate binding protein 5	−1.90	1.33
I830012O16Rik	RIKEN cDNA I830012O16 gene	−1.79	1.56
Cxcl9	Chemokine (C-X-C motif) ligand 9	−1.75	1.44
Mx1	Myxovirus (influenza virus) resistance 1	−1.66	1.44
Pydc4	Pyrin domain containing 4	−1.64	1.56
Cd69	CD69 antigen	−1.63	1.37
Olfr56	Olfactory receptor 56	−1.62	1.56
Ifi204	Interferon activated gene 204	−1.55	1.56
Tfpi2	Tissue factor pathway inhibitor 2	−1.54	1.56
Irgm1	Immunity-related GTPase family M member 1	−1.53	1.56
Selp	Selectin, platelet	−1.50	1.34
Gbp3	Guanylate binding protein 3	−1.48	1.44
Gm4951	Predicted gene 4951	−1.45	1.50
Il18rap	Interleukin 18 receptor accessory protein	−1.45	1.32
Egln3	EGL nine homolog 3 (*C. elegans*)	−1.40	1.56
Igtp	Interferon gamma induced GTPase	−1.40	1.56
Ceacam10	Carcinoembryonic antigen-related cell adhesion molecule 10	−1.39	1.47
Rnd1	Rho family GTPase 1	−1.39	1.39
Mmp25	Matrix metallopeptidase 25	−1.37	1.31
Gm12250	Predicted gene 12250	−1.37	1.31
Gapt	Grb2-binding adaptor, transmembrane	−1.36	1.31
Slc26a4	Solute carrier family 26, member 4	−1.35	1.42
Usp18	Ubiquitin specific peptidase 18	−1.35	1.56
Tgm1	Transglutaminase 1, K polypeptide	−1.34	1.50
Fgf23	Fibroblast growth factor 23	−1.32	1.39
Ifi203	Interferon activated gene 203	−1.31	1.56
Cd274	CD274 antigen	−1.31	1.44
Endou	Endonuclease, poly(U) specific	−1.30	1.33
Cxcl5	Chemokine (C-X-C motif) ligand 5	−1.29	1.52
Parp14	Poly(ADP-ribose) polymerase family, member 14	−1.29	1.56
Inhba	Inhibin beta-A	−1.29	1.56
Cmpk2	Cytidine monophosphate (UMP-CMP) kinase 2, mitochondrial	−1.28	1.56
Dhx58	DEXH (Asp-Glu-X-His) box polypeptide 58	−1.27	1.56
Ifi47	Interferon gamma inducible protein 47	−1.24	1.44
Plaur	Plasminogen activator, urokinase receptor	−1.24	1.33
Rtp4	Receptor transporter protein 4	−1.23	1.33
Slfn9	Schlafen 9	−1.20	1.56
Ccl11	Chemokine (C-C motif) ligand 11	−1.20	1.50
Mnda	Myeloid cell nuclear differentiation antigen	−1.19	1.50
Gbp2	Guanylate binding protein 2	−1.18	1.36
Adamts4	ADAMTS type 1 motif, 4	−1.17	1.33
Il2ra	Interleukin 2 receptor, alpha chain	−1.17	1.56
D14Ertd668e	DNA segment, Chr 14, ERATO Doi 668, expressed	−1.16	1.56
Tnfaip6	Tumor necrosis factor alpha induced protein 6	−1.15	1.46
Rnf213	Ring finger protein 213	−1.14	1.56
Slfn8	Schlafen 8	−1.14	1.44
Amica1	Adhesion molecule, interacts with CXADR antigen 1	−1.13	1.44
Oas1g	2'-5' Oligoadenylate synthetase 1G	−1.13	1.44
Tslp	Thymic stromal lymphopoietin	−1.13	1.44
Mir155	MicroRNA 155	−1.11	1.46
Pydc3	Pyrin domain containing 3	−1.11	1.56
Tap1	Transporter 1, ATP-binding cassette, subfamily B (MDR/TAP)	−1.08	1.56
Mcoln2	Mucolipin 2	−1.08	1.33

(Continued on next page)

TABLE 1 (Continued)

Abbreviation	Name	Log_2(FC)	$-Log_{10}$(FDR)
Hcn4	Hyperpolarization-activated, cyclic nucleotide-gated K^+ 4	−1.06	1.33
Gm12185	Predicted gene 12185	−1.04	1.33
Eif2ak2	Eukaryotic translation initiation factor 2-alpha kinase 2	−1.04	1.56
Ifi44	Interferon-induced protein 44	−1.03	1.50
Gyk	Glycerol kinase	−1.03	1.44
Parp9	Poly (ADP-ribose) polymerase family, member 9	−1.01	1.56
Ifi205	Interferon activated gene 205	−1.01	1.53
Gata2	GATA binding protein 2	1.02	1.46
Atp7b	ATPase, Cu^{2+} transporting, beta polypeptide	1.09	1.56
Anpep	Alanyl (membrane) aminopeptidase	1.12	1.56
Adamts15	ADAMTS type 1 motif, 15	1.72	1.56
Etv5	ETS variant gene 5	1.77	1.56

[a]$Log_2(FC) > 1.0$ and < -1, FDR < 0.05. Genes in boldface are present in both Tables 1 and 2.

a dysregulated immune state and that while there is induction of inflammatory repressors, their action is not sufficient to overcome other signaling pathways.

To confirm these findings using a complementary *in silico* method, we analyzed the data using Gene Set Enrichment Analysis (GSEA) (16, 17). All genes on the Mouse Gene 1.0 ST array were ranked by moderated *t* statistic for anti-OSM versus control IgG. This list was compared with a collection of gene sets from the Molecular Signatures Database (version 4.0) to determine whether members of a given gene set were distributed nonrandomly within the ranked list. Results in Table 3 indicate the top 20 gene sets upregulated and downregulated (by normalized enrichment score, or NES). Again, we see that there is a strong representation of pathways associated with interferon signaling and innate immunity downregulated with OSM neutralization. Interestingly, by this analysis there is also a significant upregulation of pathways associated with metabolism.

Exogenous OSM directly stimulates multiple inflammatory pathways in the lungs. Acute bacterial pneumonia has been shown to activate multiple redundant innate immune signaling pathways in the lungs (4), and teasing apart the effect of changing a single cytokine in this setting can be difficult. To examine the effect of OSM on the lung using a more direct approach, we investigated the effect of recombinant mouse OSM (rmOSM) stimulation on transcription factor activation. Mice were intratracheally (i.t.) instilled with 2.5 μg rmOSM and harvested for total protein after 1 h, and immunoblotting was performed (whole-blot images are available in Fig. S1 in the supplemental material). We first examined the impact of exogenous OSM on the transcription factors STAT1 and STAT3, as they are known to be induced by OSM signaling in multiple disease models (12, 18–21) and were strongly predicted by our bioinformatics results described above. Stimulation with rmOSM resulted in the activation of STAT1 and STAT3 (Fig. 3), as evidenced by an increase in phosphoprotein (Fig. 3A and D) and phosphoprotein to total protein ratio (Fig. 3C and F). Interestingly, IRF3, which is an interferon-regulated transcription factor strongly predicted by our array to be decreased (Fig. 1D), was not activated by exogenous rmOSM (Fig. 3J and Fig. S1). We next looked at the upstream regulator AKT, which has been shown in other models to be affected by OSM in the lungs (22–26). Interestingly, there was a trend toward diminished phospho-AKT (Fig. 3G), and a significant decrease in the ratio of phosphoprotein to total protein (Fig. 3I), without changes in total AKT (Fig. 3H). This suggests that AKT is regulated differently from STAT1 and STAT3 by rmOSM in our model. Taken together, these data suggest that OSM directly modulates multiple immune signaling pathways in the lungs, which is consistent with the results from our transcriptomic studies.

We next determined whether OSM alone was sufficient to elicit gene expression changes implicated by differentially expressed transcripts (Fig. 1 and 2 and Tables 1 and 2) following anti-OSM during pneumonia. Mice were treated with an i.t. instillation of rmOSM for 4 h, and mRNA induction was measured for select transcripts using quantitative reverse transcription-PCR (qRT-PCR) (Fig. 4). We first evaluated *Csf3*, *Saa1*, *Selp*,

TABLE 2 DEG predicted to be downstream of OSM

Genes[a]	Name	Log_2(FC)	$-Log_{10}$(FDR)	Predicted regulation
Csf3	Colony stimulating factor 3 (granulocyte)	−1.96	1.56	Up
Il6	Interleukin 6	−1.94	1.02	Up
Saa1	Serum amyloid A 1	−1.90	1.46	Up
Selp	Selectin, platelet	−1.50	1.34	Up
Ccl2	Chemokine (C-C motif) ligand 2	−1.31	1.11	Up
Sele	Selectin, endothelial cell	−1.25	1.11	Up
Ccl11	Chemokine (C-C motif) ligand 11	−1.20	1.50	Up
Cxcl10	Chemokine (C-X-C motif) ligand 10	−1.20	1.05	Up
Gbp2	Guanylate binding protein 2	−1.18	1.36	Up
Adamts4	ADAMTS type 1 motif, 4	−1.17	1.33	Regulates
Irf7	Interferon regulatory factor 7	−1.13	1.22	Up
Oas1g	2'-5' Oligoadenylate synthetase 1G	−1.13	1.44	Up
Tap1	Transporter 1, ATP-binding cassette, subfamily B (MDR/TAP)	−1.08	1.56	Up
Timp1	Tissue inhibitor of metalloproteinase 1	−0.92	1.29	Up
Sbno2	Strawberry notch homolog 2 (*Drosophila*)	−0.84	1.56	Up
Tlr2	Toll-like receptor 2	−0.80	1.09	Up
Casp4	Caspase 4, apoptosis-related cysteine peptidase	−0.79	1.05	Up
Irf9	Interferon regulatory factor 9	−0.78	1.06	Up
Ch25h	Cholesterol 25-hydroxylase	−0.77	1.41	Up
Socs1	Suppressor of cytokine signaling 1	−0.72	1.33	Up
Zc3hav1	Zinc finger CCCH type, antiviral 1	−0.71	1.19	Up
Hif1a	Hypoxia-inducible factor 1, alpha subunit	−0.68	1.27	Up
Ptges	Prostaglandin E synthase	−0.66	1.22	Up
Il17a	Interleukin 17A	−0.65	1.02	Down
Myd88	Myeloid differentiation primary response gene 88	−0.61	1.05	Up
Irf1	Interferon regulatory factor 1	−0.60	1.02	Up
Znf263	Zinc finger protein 263	−0.58	1.16	Up
Ifi35	Interferon-induced protein 35	−0.52	1.32	Up
Pdzk1ip1	PDZK1-interacting protein 1	−0.51	1.22	Up
Pfkfb3	6-Phosphofructo-2-kinase/fructose-2,6-biphosphatase 3	−0.49	1.10	Up
Crp	C-reactive protein, pentraxin-related	−0.48	1.01	Regulates
Dhrs7	Dehydrogenase/reductase (SDR family) member 7	−0.43	1.06	Up
Tlr3	Toll-like receptor 3	−0.42	1.05	Up
Hla-a	Histocompatibility 2, Q region locus 6	−0.40	1.12	Up
Il4r	Interleukin 4 receptor, alpha	−0.39	1.09	Up
Col8a1	Collagen, type VIII, alpha 1	−0.37	1.00	Up
Zhx2	Zinc fingers and homeoboxes 2	−0.37	1.00	Up
Stk25	Serine/threonine kinase 25 (yeast)	0.33	1.00	Down
Rnase4	Ribonuclease, RNase A family 4	0.40	1.11	Down
Prdx2	Peroxiredoxin 2	0.42	1.18	Down
Rora	RAR-related orphan receptor alpha	0.46	1.09	Down
Ryk	Receptor-like tyrosine kinase	0.47	1.28	Up
Irs1	Insulin receptor substrate 1	0.53	1.31	Down
Gab1	Growth factor receptor bound protein 2-associated protein 1	0.58	1.10	Up
Dapk1	Death associated protein kinase 1	0.59	1.11	Up
Znf266	Zinc finger protein 266	0.73	1.09	Up
Erbb3	v-erb-b2 erythroblastic leukemia viral oncogene homolog 3	0.81	1.56	Down
Dhrs3	Dehydrogenase/reductase (SDR family) member 3	0.97	1.44	Down

[a]Genes in boldface are present in both Tables 1 and 2.

and *Adamts4*, as they were all listed as OSM-related genes in the IPA Knowledge Base and were highly significant. *Saa1* and *Adamts4* were both strongly induced by rmOSM, while *Csf3* and *Selp* only trended toward a modest increase. We next looked at several interferon-related DEG (*Ifit1-3* and *Cxcl9*) that were highly significant yet not listed as being downstream of OSM. In contrast to what was predicted by our array data, *Ifit2* and *Ifit3* were significantly decreased with rmOSM treatment, while *Ifit1* trended lower. *Cxcl9* only trended modestly up after rmOSM treatment. Among genes induced by OSM neutralization, we examined *Etv5*, *Anpep*, and *Gata2*, all of which were highly significant though not previously shown to be OSM associated. After rmOSM treatment, there was a significant decrease in *Etv5* and *Gata2* and a trend toward decrease with *Anpep*, all of which is consistent with the predictions. These results demonstrate that

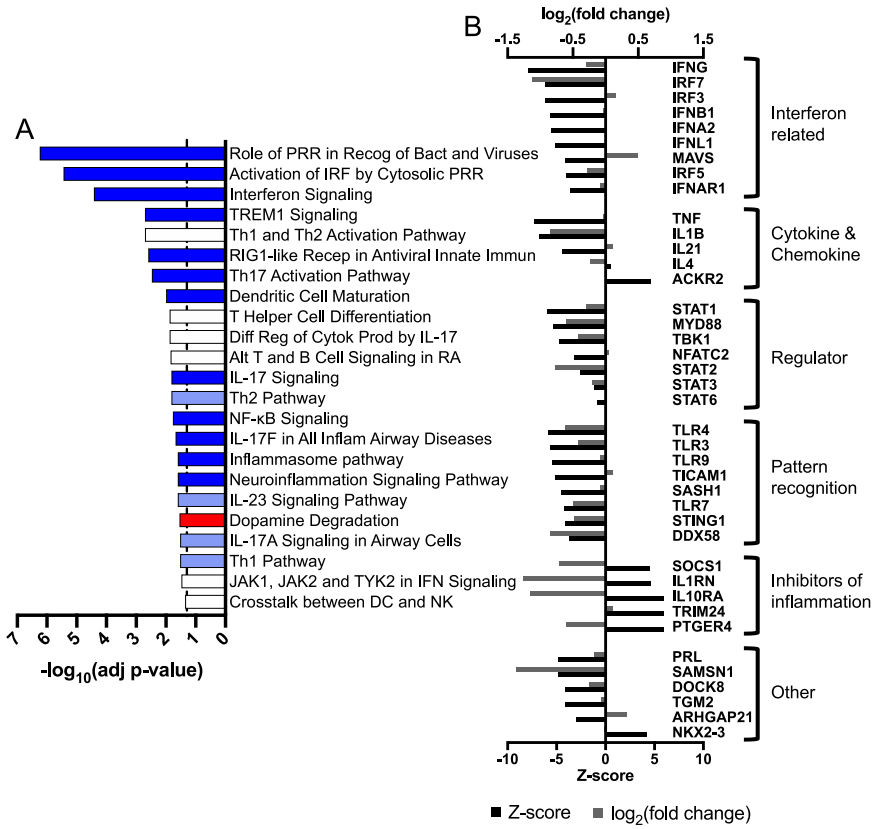

FIG 2 Predicted pathways and upstream regulators affected by OSM blockade. (A) Canonical pathways as predicted by Ingenuity Pathway Analysis (IPA). Bars colored based on z-score (dark blue, <-1; light blue, between -1 and 0; white, 0; and red, >1 [no z-score between 0 and 1]). Significance was determined by Benjamini Hochberg multiple testing correction of *P* value; vertical dotted line represents $-\log_{10}$(adjusted *P* value) of 1.3. (B) Top 40 upstream regulators affected by OSM neutralization, as predicted by IPA. Each regulator is presented with the z-score (black bar, bottom axis) and the $\log_2$(fold change) of expression of the gene (gray bar, top axis). Regulators are organized by function and in decreasing order of z-score. For the presented regulators, *P* values of overlap ranged from 4.87×10^{-37} to 5.80×10^{-13}.

not all genes significantly changed by OSM neutralization during pneumonia are changed as predicted with OSM stimulation (without pneumonia). Especially notable are the *Ifit* genes, which change opposite to what was predicted by the array results. In this case, while OSM may be capable of suppressing these genes in the absence of infection, the combination of circumstances secondary to the impact of OSM neutralization during pneumonia overwhelm the direct effects of OSM observable for select transcripts. For the other genes investigated, OSM is independently sufficient to induce gene expression programs that are reduced following OSM blockade during pneumonia.

Neutralization of OSM leads to a rebalancing of late inflammatory signaling. As the studies described above address OSM-dependent pathways in the initial 1 to 6 h of infection, we next determined the impact of OSM blockade on transcription factor activity at 24 h, a time by which we previously reported changes in immune function (12, 13, 27). To do this, we infected mice for 24 h with *E. coli* in the presence of IgG or neutralizing anti-OSM antibody, isolated total lung protein, and performed immunoblotting (whole-blot images of blots available in Fig. S2). Interestingly, and in contrast to exogenous OSM after 1 h, neutralization of OSM during pneumonia increased activated phospho-STAT1 (Fig. 5A) and the ratio of pSTAT1/STAT1 (Fig. 5C). On the other hand, the fraction of active phospho-STAT3 (Fig. 5D and F) became elevated due largely to a decrease in total STAT3 (Fig. 5E). Taken together, these data suggest that neutralization of OSM leads to alteration in the typical balance of STAT1 and -3 activity seen in

TABLE 3 GSEA most up- and downregulated gene sets

Gene set name	Gene set size[a]	NES	$-Log_{10}$(FDR)	Group
Interferon alpha beta signaling	42	−3.09	>4.05	Reactome pathway
Interferon signaling	117	−3.01	>4.05	Reactome pathway
Interferon gamma signaling	48	−3.00	>4.05	Reactome pathway
Cytokine signaling in immune system	221	−2.81	>4.05	Reactome pathway
Olfactory signaling pathway	230	−2.74	>4.05	Reactome pathway
Olfactory transduction	286	−2.68	>4.05	KEGG pathway
Defense response	218	−2.67	>4.05	GO biological process
Cytokine production	65	−2.54	>4.05	GO biological process
Cytokine-cytokine receptor interaction	215	−2.50	>4.05	KEGG pathway
Interleukin binding	24	−2.46	>4.05	GO molecular function
Class a1 rhodopsin like receptors	270	−2.44	>4.05	Reactome pathway
Inflammatory response	116	−2.41	>4.05	GO biological process
Immune response	203	−2.40	>4.05	GO biological process
JAK STAT signaling pathway	132	−2.37	>4.05	KEGG pathway
Defense response to bacterium	19	−2.37	>4.05	GO biological process
Cytokine activity	81	−2.32	3.95	GO molecular function
Detection of stimulus	45	−2.32	3.97	GO biological process
Response to bacterium	24	−2.32	4.00	GO biological process
Cytokine metabolic process	40	−2.32	4.02	GO biological process
IL-22bp pathway	16	−2.32	4.04	BioCarta pathway
Valine leucine and isoleucine degradation	42	2.44	>4.05	KEGG pathway
ACTAYRNNNCCCR unknown	425	2.31	>4.05	TF Motif
Activation of chaperone genes by xbp1s	43	2.31	>4.05	Reactome pathway
Propanoate metabolism	30	2.25	>4.05	KEGG pathway
Endoplasmic reticulum part	94	2.22	3.69	GO cellular component
Asparagine N-linked glycosylation	78	2.21	3.16	Reactome pathway
Mitochondrion	318	2.19	3.22	GO cellular component
Endoplasmic reticulum	275	2.18	3.19	GO cellular component
Isomerase activity	34	2.14	2.89	GO molecular function
Major histocompatibility complex class II antigen presentation	81	2.13	2.87	Reactome pathway
Endoplasmic reticulum membrane	83	2.12	2.79	GO cellular component
Fatty acid metabolism	38	2.10	2.70	KEGG pathway
N glycan biosynthesis	44	2.10	2.68	KEGG pathway
Nuclear envelope endoplasmic reticulum network	92	2.09	2.64	GO cellular component
Golgi apparatus part	97	2.06	2.42	GO cellular component
Mitochondrial part	128	2.04	2.34	GO cellular component
Nucleotide excision repair	46	2.04	2.35	Reactome pathway
Lysosome	114	2.04	2.31	KEGG pathway
Unfolded protein response	74	2.03	2.29	Reactome pathway
Endomembrane system	213	2.02	2.26	GO cellular component

[a]Number of genes in the gene set that overlap with the genes in the ranked list.

pneumonia, yet this disruption is distinct from what was predicted by gene changes in the transcriptomic data at 6 h. We observed an increase in both phospho-AKT (Fig. 5G) and total AKT (Fig. 5H) with OSM neutralization, yet their relative ratio was unchanged (Fig. 5I). OSM blockade had no effect on IRF3 (Fig. 5J). Overall, this suggests that neutralization of OSM leads to activation of known proinflammatory signaling pathways in the lungs. While this seemingly opposes changes predicted based on data collected at earlier time points (Fig. 1 and 3), exaggerated activity of these transcription factors at 24 h may be secondary to outcomes directly altered by OSM blockade in the initial hours of infection.

OSM RNA is produced by neutrophils and macrophages. To better understand the origins of lung OSM accumulation during pneumonia, we investigated its cellular sources. We performed flow cytometry-assisted cell sorting (FACS) to isolate lung cell types and measured OSM RNA produced in each cell type with and without infection. We previously demonstrated that in the absence of infection, OSM protein is undetectable in the alveolar lining fluid but is rapidly upregulated by 6 h of *E. coli* pneumonia (13). While neutrophils have been identified by others as an OSM source in different

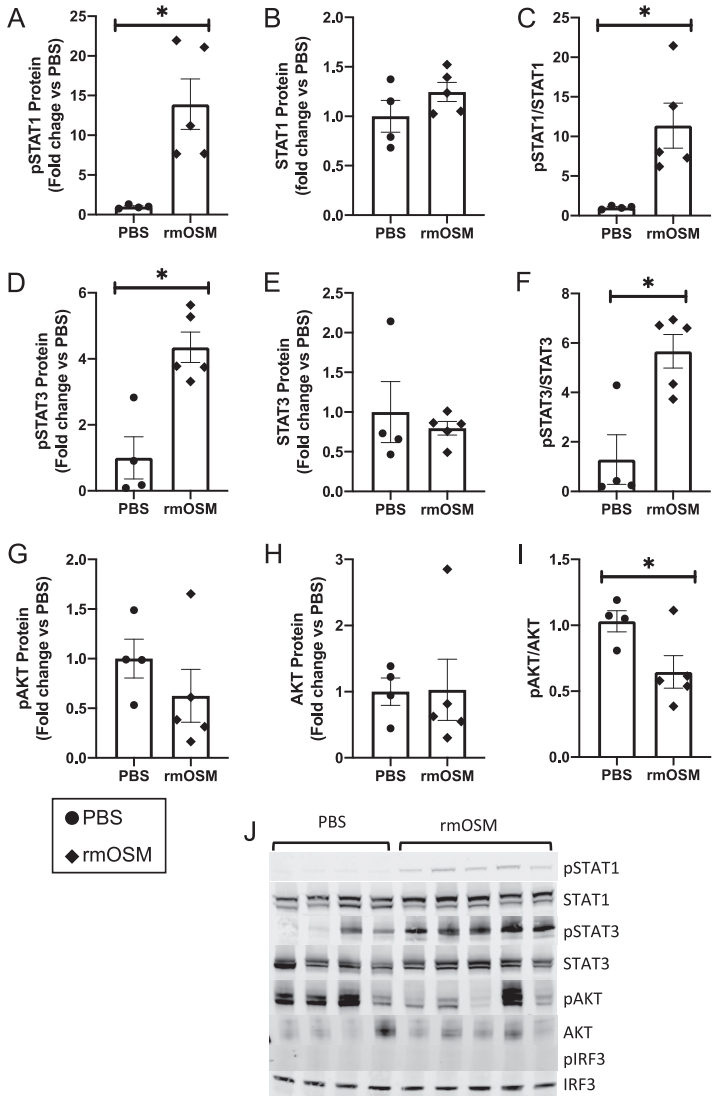

FIG 3 OSM activates multiple signaling pathways in the lungs. Mice were treated with PBS (circle, $n = 4$) or 2.5 μg rmOSM (diamond, $n = 5$) for 1 h. Protein from left lung lobes was isolated, and immunoblotting was performed for the indicated targets. Phosphoprotein (A, D, and G), total target protein (B, E, and H), and the ratio of phospho- to total protein (C, F, and I) are presented for each target. Targets are STAT1 (A to C), STAT3 (D to F), and panAKT (G to I). Immunoblots are displayed in panel J, and full blots are shown in Fig. S1. Targets were quantified using Empiria Studio, and fluorescence intensity was normalized to total protein in each lane as measured by Revert total protein stain. Values presented are fold change versus PBS control for each target or ratio of fold changes. Bars represent means, and error bars are SEM. Experiments were performed over two separate days. Equivalence of variance was checked with an F test. In sample sets with equivalent variance, significance was calculated with unpaired *t* test (STAT1, pSTAT3, pSTAT3/STAT3, and all AKT data). In sample sets with significantly different variance, significance was calculated with a Mann-Whitney test (pSTAT1, pSTAT1/STAT1, and STAT3). *, $P < 0.05$.

inflammatory settings (8, 28–30), we predicted alternative sources given our previous finding that OSM is an upstream requirement for the recruitment of neutrophils (13). We focused our initial sorting strategy on myeloid lineage cells and epithelium (sorting strategy is depicted in Fig. S3), as these cell types are first in contact with *E. coli*. Mice were treated with *E. coli* or saline control for 6 h, and peripheral blood (Fig. 6A), bronchoalveolar lavage fluid (BALF) (Fig. 6B), or whole-lung single-cell suspensions (Fig. 6C) were harvested. Cell suspensions were subjected to FACS, RNA isolation, and OSM RNA detection. Data were normalized to uninfected, whole-lung OSM RNA to relate fold

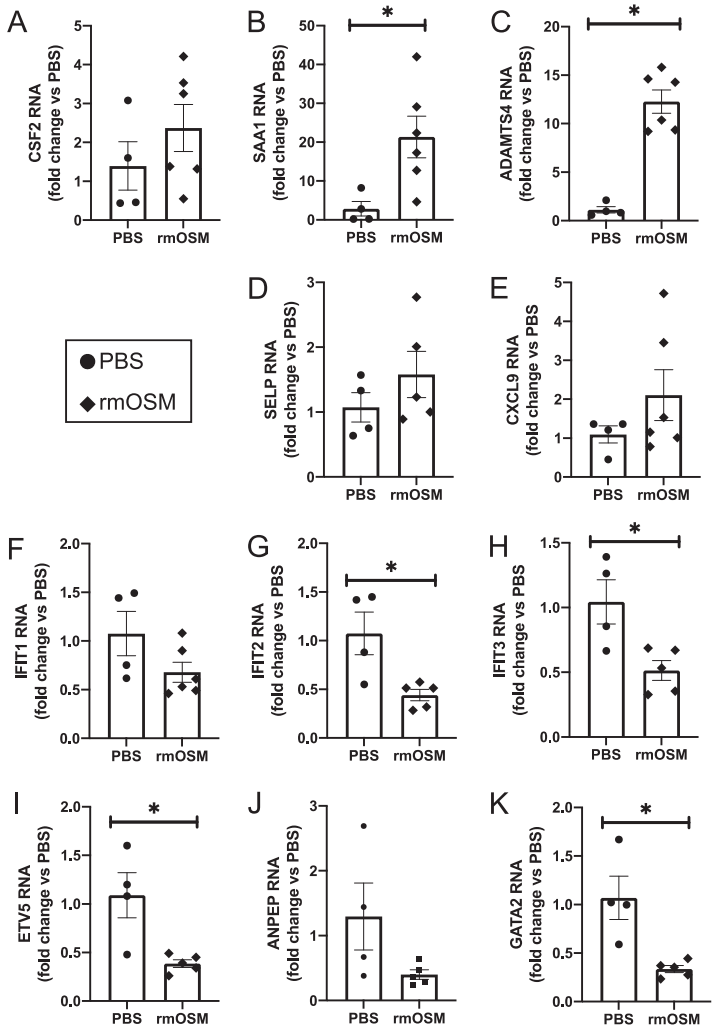

FIG 4 rmOSM alters transcription of several differentially expressed genes (DEG) from the array. Mice were treated with 50 ng rmOSM (diamond, $n = 5$ to 6) or PBS control (circle, $n = 4$) for 4 h. RNA was isolated from left lobes, and qRT-PCR was performed on the following transcripts: (A) *Gcsf*, (B) *Saa1*, (C) *Adamts4*, (D) *Selp*, (E) *Cxcl9*, (F) *Ifit1*, (G) *Ifit2*, (H) *Ifit3*, (I) *Etv5*, (J) *Anpep*, and (K) *Gata2*. Values presented are fold changes of transcript compared with PBS-treated control mice. Bars represent means, and error bars are SEM. Experiments were performed over two separate days. Equivalence of variance was checked with an F test. In sample sets with equivalent variance, significance was calculated with unpaired *t* test (*Csf2*, *Saa1*, *Selp*, *Ifit1*, *Ifit3*, *Cxcl9*, *Anpep*, and *Gata2*). In sample sets with significantly different variance, significance was calculated with Mann-Whitney test (*Adamts4*, *Ifit2*, and *Etv5*). *, $P < 0.05$.

induction values across cell types. Compared to whole-lung tissue from uninfected mice, neutrophils had high levels of OSM production, both in the peripheral blood (4,232 ± 761, fold change mean ± standard errors of the means [SEM]) and whole-lung single-cell suspension (4,452 ± 954). Lung suspension macrophages (1,101 ± 384) and other leukocytes (684 ± 77) produced moderate amounts of OSM at baseline. Peripheral blood monocytes (165 ± 35) and BALF macrophages (95 ± 7) had lower levels, and lung suspension epithelial cells (2 ± 1) had the lowest level of cells measured. Note that BALF neutrophils are rare in the absence of infection and, therefore, could not be evaluated in its absence. During infection, however, neutrophils isolated from BALF exhibited the highest OSM mRNA levels of all cell types tested (60,931 ± 18,863), while the high levels of OSM in peripheral blood (7,770 ± 2,486) and whole-lung digest (3,004 ± 735) neutrophils did not change significantly with infection. OSM mRNA levels

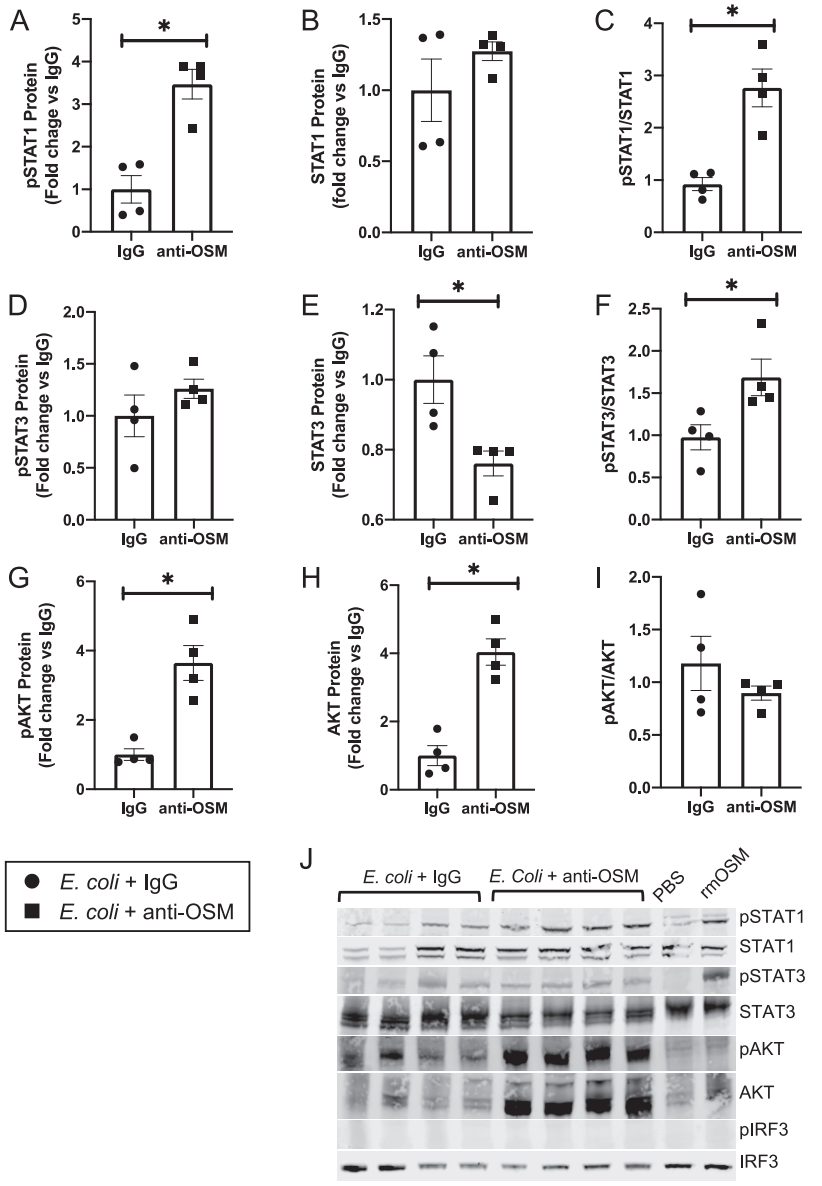

FIG 5 OSM neutralization leads to activation of STAT1. Mice were infected with *E. coli* and IgG control (circle, $n = 4$) or anti-OSM (square, $n = 4$) for 24 h. Protein from left lung lobes was isolated, and immunoblotting was performed for the indicated targets. Phosphoprotein (A, D, and G), total target protein (B, E, and H), and the ratios of phospho- to total protein (C, F, and I) are shown for each target. Targets are STAT1 (A to C), STAT3 (D to F), and panAKT (G to I). Immunoblots are displayed in panel J, and full blots are shown in Fig. S2. Targets were quantified using Empiria Studio, and fluorescence intensity was normalized to total protein in each lane. Values presented are fold change versus PBS control for each target. Bars represent means, and error bars are SEM. Experiments were performed over two separate days. Equivalence of variance was checked with an F test, and all sets had equivalent variance. Significance was calculated with unpaired *t* test. *, $P < 0.05$.

in peripheral blood monocytes (2,770 ± 386) and BALF macrophages (1,289 ± 323) were higher during infection than at baseline, although this did not reach statistical significance. Macrophages (585 ± 68) and other leukocytes (553 ± 234) in the lung suspension had slightly lower levels of OSM during infection than at baseline, but again this did not reach significance. Finally, lung suspension epithelial cells (9 ± 3) had the lowest level measured during infection. These data suggest that neutrophils overall, particularly in the alveolar space (BALF neutrophils), are the predominant source of

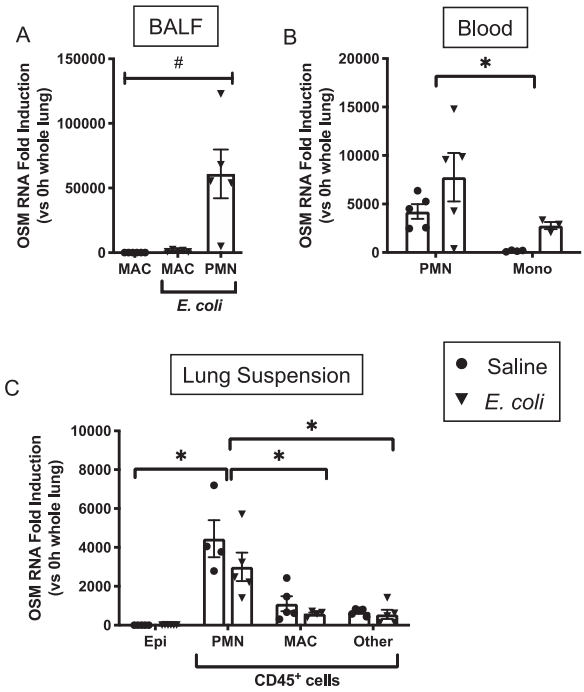

FIG 6 OSM is produced by neutrophils, monocytes, and macrophages. Mice were i.t. instilled with either saline control (circles, $n = 4$ to 6) or *E. coli* (inverted triangles, $n = 4$ to 6). After 6 h, BALF cells (A), peripheral blood cells (B), or whole-lung single-suspension cells (C) were isolated. FACS was performed to isolate alveolar or whole-lung macrophages (MAC; A and C), alveolar, peripheral blood, or whole-lung neutrophils (PMN; A to C), peripheral blood monocytes (Mono; B), whole-lung epithelial cells (Epi; C), or whole-lung nonmacrophage, nonneutrophil leukocytes (Other; C). RNA was harvested from sorted cells, and OSM RNA was determined. Values presented are fold induction of OSM compared to uninfected, whole lung. Bars represent means, and error bars are SEM. For panel A, significance was determined by Kruskal-Wallis one-way analysis of variance (ANOVA), with Dunn correction for multiple testing. #, $P < 0.05$. For panels B and C, significance was determined by two-way ANOVA with Sidak correction for multiple testing. *, $P < 0.05$ for effect of cell type. Of note, there was no significant effect of infection in any cell type.

OSM RNA at baseline, with infections with macrophages, monocytes, and other leukocytes serving as potential secondary sources.

Macrophages and neutrophils produce OSM protein in the lungs. We next looked at OSM protein production at baseline and following 6 h of lung infection. Figure 7A demonstrates that F4-80 colocalizes with OSM staining, both at baseline and with infection, revealing macrophages as a source of OSM protein, with more prominent staining detected during infection. Figure 7B shows that Ly6G also colocalizes with OSM at baseline and during pneumonia. The neutrophils at baseline appear to be largely confined to the circulation in the alveolar septa. During infection, there are more neutrophils, found both in the septa as well as the alveolar space, suggesting neutrophils as a recruited source of OSM complementing an additional response from resident macrophages. Overall, our findings support neutrophils and macrophages as major OSM sources in the lungs.

Macrophages are sufficient but not necessary for OSM production. In our model system, neutrophil recruitment to the alveolar space requires alveolar OSM (13), as neutralization of alveolar OSM during pneumonia limits neutrophil recruitment. In an uninfected state, there are few to no neutrophils in the alveolar space, suggesting another cell type is involved in early OSM signaling. We hypothesized that an early signaling cell is the alveolar macrophage, which functions as a sentinel cell in the alveolus (4). We investigated whether alveolar macrophages were able to rapidly produce OSM by treating mice with *E. coli* for 2 h. We confirmed by differential staining of cytospin slides that cells harvested from the BALF of mice at 2 h were comprised of greater than 99% alveolar macrophages (Fig. 8A). We next harvested RNA from these cells and

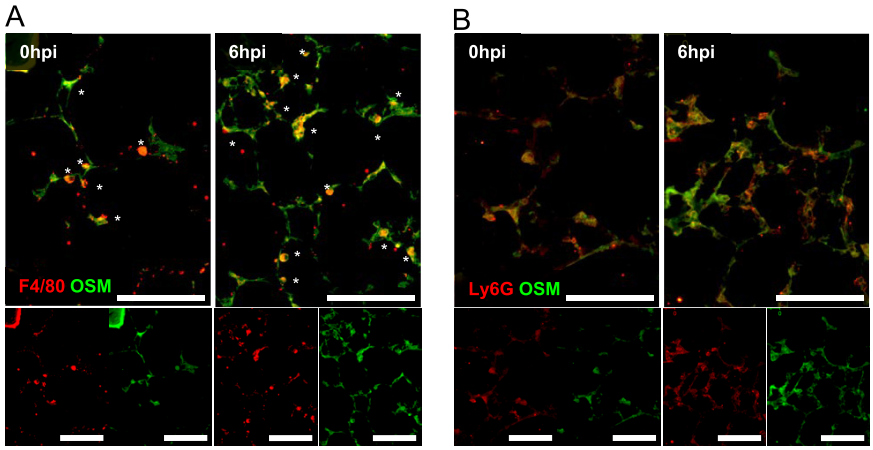

FIG 7 Macrophage and neutrophil staining colocalizes with OSM staining during pneumonia. Mice were i.t. instilled with *E. coli*, and involved left lobes were harvested at baseline (0 hpi) or after 6 h (6 hpi). Frozen sections were obtained and stained for OSM (green) plus either F4/80 (A) or Ly6G (red) (B). Micrographs are representative images; magnification, ×400. White scale bars represent 75 μm.

evaluated OSM production. Compared to cells from uninfected mice, those collected after 2 h of *E. coli* infection exhibited substantial OSM induction (Fig. 8B). This suggests alveolar macrophages as an early source of OSM.

To determine whether early mRNA induction in alveolar macrophages is required for the total lung OSM response, we depleted airspace macrophages by pretreating mice with clodronate-encapsulated liposomes, which resulted in approximately 75% reduction in BALF macrophages (samples collected in reference 31). When these mice were infected for 6 or 24 h with *E. coli*, there was no significant decrease in OSM produc-

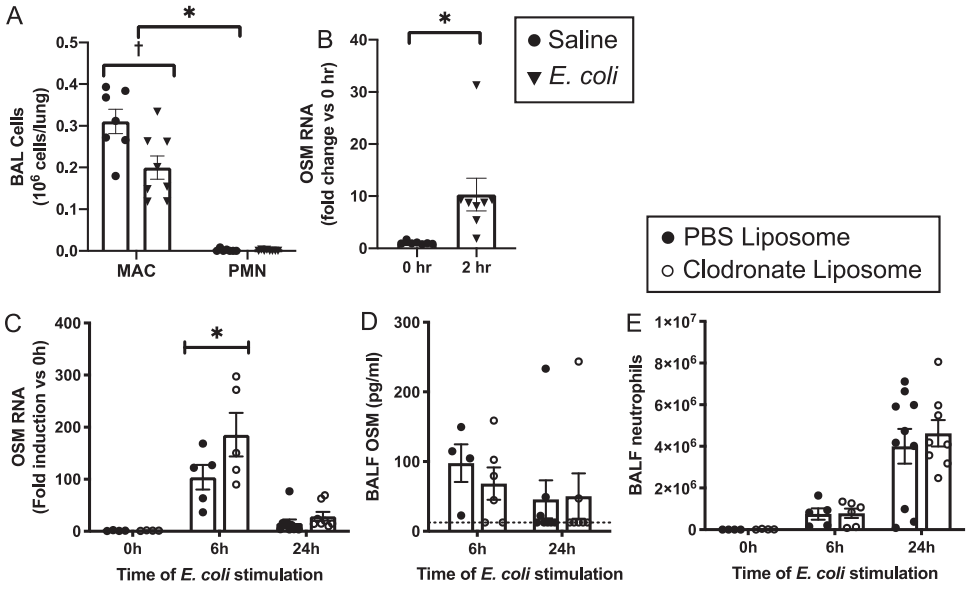

FIG 8 Macrophages are sufficient but not necessary to produce OSM. (A and B) Mice were i.t. instilled with *E. coli*, and BALF cells were harvested at baseline (circles, $n = 7$) or after 2 h of infection (inverted triangle, $n = 8$), and differential cell counts (MAC macrophage and PMN neutrophils) (A) and OSM RNA levels (B) were determined. For panel A, significance was determined by two-way ANOVA with Sidak correction for multiple testing. †, $P < 0.05$ for effect of infection; *, $P < 0.05$ for effect of cell type. For panel B, significance was determined by Mann-Whitney test, as variance was significantly different between sets. *, $P < 0.05$. For panels C to E, mice were treated with clodronate liposomes (open circles) or control PBS liposomes (closed circles) for 72 h, and then mice were i.t. infected with *E. coli* for 6 or 24 h. (C) Left lobe was harvested to measure RNA OSM. BALF was collected to measure OSM protein (D) or total neutrophil counts (C). Significance was tested with two-way ANOVA with Sidak correction for multiple comparisons. *, $P < 0.05$.

tion at either the RNA (Fig. 8C) or protein (Fig. 8D) level. In fact, there was a significant increase in OSM RNA production at 6 h in the clodronate-treated mice, perhaps secondary to other altered pneumonia outcomes following macrophage depletion. Furthermore, there was no change in neutrophil recruitment with clodronate treatment (Fig. 8E). These data suggest that while macrophages produce OSM quite early in response to infection, alternative cell types, such as neutrophils, are the early source of OSM prior to the arrival of additional (OSM-dependent) neutrophils into the alveolar space.

DISCUSSION

We have shown that OSM plays an important role in pneumonia, regulating several aspects of early innate immune signaling. This modulation appears to be quite complex. Direct OSM stimulation results in the induction of proinflammatory signaling, but in the absence of OSM, there is also a rebalancing of inflammatory signaling pathways associated with increased mortality. While there have been several studies examining pulmonary OSM in fibrotic models of lung disease, this study is the first to examine how OSM affects localized inflammatory signaling pathways during pneumonia. Furthermore, we have confirmed neutrophils and macrophages, particularly the former, as important producers of pulmonary OSM.

While we are the first group to examine the effect of OSM neutralization on mortality during pneumonia, we are not the first to evaluate this outcome in mouse models of infection. Others have shown that OSM blockade reduces mortality in a cecal ligation and puncture model of sepsis, whereas the opposite result occurred following exogenous OSM administration (7). However, others have shown that OSMr$^{-/-}$ mice (OSM receptor-null mice) have decreased survival after intestinal ischemia-reperfusion injury, likely secondary to intestinal sepsis (32). Thus, the influence of OSM in inflammatory settings appears to be complex and context dependent. These two studies unequivocally reveal the functional relevance of OSM, but they also highlight the difficulty of using mortality as an endpoint, as does our own report. An important distinction of our approach with pneumonia models is our strategy for localized OSM neutralization in the airspaces, which confines the setting in which its contributions are being interrogated.

Using microarray analysis after only 6 h of infection, we identified several signaling pathways that are predicted to be affected by OSM during pneumonia, including STAT1, STAT3, type I and II interferon, and TH17. While we could demonstrate direct effects of exogenous OSM on some of these factors following 1 h of stimulation (namely, STAT1 and STAT3), we did not see a significant decrease in their activation after OSM neutralization following 24 h of pneumonia. In fact, STAT1 and STAT3 were both induced with OSM neutralization. A possible explanation for these results is that many of the innate immune signaling pathways in the lungs are redundant, and neutralization of a single cytokine results in compensatory activation of other pathways. However, this compensation may not be quite as effective as the original cytokine, resulting in an overabundant immune response. Additionally, increases in STAT1 and STAT3 may reflect the manifestation of other complications following OSM deficiency. Indeed, such complications are severe enough to result in early mortality (Fig. 1A), suggesting that immune alterations observed by 24 h (e.g., elevated STAT1/3) could be secondary to earlier damaging events. An alternate hypothesis is that the neutralizing ability of our anti-OSM antibody wanes over time, making way for a later wave of OSM production (along with changes to other STAT1/3-activating factors) to elicit an even stronger STAT1/3 response downstream of OSM blockade. However, we previously measured OSM in BALF in a similar anti-OSM *E. coli* model (13) and observed significant blockade of OSM detection in the airspaces through at least 48 h of infection. As discussed below, however, it is possible that cells produce OSM outside the alveolar space, which could contribute to STAT1/3 activation (detected in lung tissue homogenates) later during an infection. In aggregate, it is clear that maintenance and regulation of STAT1 and STAT3 are influenced by OSM during pneumonia. This possibility is

consistent with others' findings from more sustained, long-term lung fibrosis models (11, 33, 34).

Interferon-related pathways were prominently represented in our transcriptional profiling data as those affected by OSM, but the degree to which these responses are mechanistically linked to OSM-mediated outcomes is presently unclear. OSM manipulation modified the activation status of STAT1, which is a critical intermediate for IFN-dependent gene expression (35). However, changes in these pathways could be secondarily related to changes in lung cellularity, particularly neutrophils, following OSM blockade. Counter to this hypothesis is that we have previously shown similar neutrophil counts in anti-OSM-treated mice at the time point selected for our transcriptional profiling studies (6 h) (13). Another possibility is that potential roles of IFN-related pathways are more consequential in the setting of viral pneumonia, paving the way for newly developing work in our laboratory distinguishing effects of OSM modulation in response to influenza. Others have shown that OSM and interferon potentiate downstream activation of STAT1 and STAT3 in liver cells (18), but whether OSM directly impacts interferon signaling in that model or in the lungs is unclear.

Another major goal of our present study was to determine prominent cellular sources of pneumonia-induced OSM in the lungs. Previous studies have shown that OSM can be made by a variety of stimulated cells, including lymphocytes (36), monocyte/macrophages (37), antigen-presenting cells (10), neutrophils (8), smooth muscle cells (38), and endothelial cells (39). However, in human studies of acute and chronic inflammatory conditions, neutrophils appear to be a primary source of OSM (28–30). Here, we show that both neutrophils and macrophages can produce OSM in the lungs. We initially hypothesized that macrophages are a very early source of OSM, which was supported by data showing alveolar macrophages upregulated OSM RNA at 2 h of infection (Fig. 8B). However, clodronate-induced macrophage depletion failed to reduce total OSM accumulation and did not affect neutrophil recruitment kinetics, suggesting greater contributions from neutrophils and/or alternative macrophage populations (i.e., recruited or interstitial, which are protected from clodronate depletion), at least at the selected time points of 6 and 24 h. In the case of neutrophils, this finding introduces an interesting feedback circuit in which recruited cells produce OSM to facilitate and maintain further neutrophil accumulation, as evidenced by diminished alveolar neutrophilia following OSM blockade (13). It is plausible that an initial wave of OSM-independent neutrophil recruitment precedes an increase in alveolar OSM concentrations followed by a subsequent OSM-mediated neutrophil response. Alternatively, OSM production by the marginated pool of blood neutrophils in the lungs may facilitate neutrophil emigration immediately after the onset of infection. This is less likely given the involvement of CXCL5, which is triggered by OSM in epithelial cells on the apical surface of the lung (13, 40). However, basolateral roles for neutrophil-derived OSM in the blood would not be unprecedented based on a recent report from Setaidi et al. (41), in which OSM from neutrophils enhanced adhesion to endothelial cells through modulation of p-selectin. Our data partially support this hypothesis in that p-selectin mRNA (SELP) was decreased in our transcriptional profiling experiment following OSM neutralization (Table 1). Furthermore, it is unclear whether selectin-mediated adhesion is a central pathway for neutrophil extravasation during pneumonia (42). However, investigation of how neutrophil-mediated OSM signaling affects neutrophil recruitment in the lungs is under active investigation.

Here, we have identified potential sources of OSM during pneumonia, along with the scope of its biological activity in the lungs, that are necessary for survival. Further studies are needed to elucidate precise mechanisms of OSM-driven signaling and protection in pneumonia. Given the complexity of the model system, it is likely that multiple distinct cell types and parallel signaling events are involved, perhaps revealing the identity of targetable pathways for clinical interventions, particularly those associated with neutrophil and immune dysfunction.

MATERIALS AND METHODS

Experimental mice. Murine experiments were carried out in C57BL/6J mice, purchased from Jackson Laboratory (Bar Harbor, ME). All experimental mice were cohoused at Boston University's animal facility, and all animal protocols were approved by the Boston University Institutional Animal Care and Use Committee (IACUC PROTO201800710). Mice were between 6 and 12 weeks old, with equal combinations of male and female mice used. All experiments had a minimum of $n = 3$ per experimental group, and experiments were repeated over 2 days, performed at the same time of day. The specific numbers of mice used in each experimental group are indicated in the figures.

i.t. instillations and pneumonia model. Prior to intratracheal (i.t.) instillation, mice were anesthetized via intraperitoneal (i.p.) injection of ketamine (50 mg/kg of body weight) and xylazine (5 mg/kg). The trachea was surgically exposed, and a 24-guage angiocatheter was inserted into the trachea and advanced to the left bronchus to direct instillations to the left lobe of the lung. All instillations were introduced in a total volume of 50 μl. Additional details on specific agents instilled are below. Instillates included *Escherichia coli*, anti-OSM neutralizing antibody (anti-OSM), IgG control, recombinant mouse OSM (rmOSM), or vehicle only. For all experiments, mice with weight loss of >20% of initial body weight or that became moribund were euthanized.

***In vivo* reagents.** Pneumonia was induced by the instillation of approximately 1×10^6 to 2×10^6 CFU *E. coli* (serotype 06:K2:H1; American Type Culture Collection [ATCC] no. 19138) in saline or phosphate-buffered saline (PBS) vehicle. We chose *E. coli* as the experimental pathogen for two main reasons. First, *E. coli* and other enteric Gram-negative bacilli are important causes of community- and health care-associated pneumonia (3, 43–45). Second, in several studies, including studies related to OSM function, we have shown that our murine model of *E. coli* pneumonia results in significant inflammation without overly high rates of mortality (12, 13, 27, 31, 40, 46, 47). For OSM neutralization experiments, *E. coli* was coinstilled with either a polyclonal goat anti-OSM neutralizing antibody (AF-495, 10 ng; anti-OSM; R&D Systems) or goat IgG control (AB-108-C, 10 ng; R&D Systems). We have previously shown that this dose of anti-OSM can block OSM-induced STAT3 activation in mouse lungs (13). For OSM supplementation experiments, rmOSM (2.5 μg or 50 ng; R&D Systems) or vehicle only (PBS) was instilled.

Microarray analysis. RNA was extracted from whole-lung homogenates as described below. RNA concentration and purity were determined using an Agilent Bioanalyzer (Agilent, Santa Clara, CA). Only samples with and RNA integrity number (RIN) of >8.0 were used. Microarray analysis was performed on an Affymetrix GeneChip platform with GeneChip Mouse Gene 1.0 (Affymetrix, Santa Clara, CA). To minimize potential batch effects, all 6 microarrays were processed together. Affymetrix GeneChip Mouse Gene 1.0 ST CEL files were normalized to produce gene-level expression values using the implementation of the Robust Multiarray Average (RMA) (48) in the affy package (version 1.36.1) (49) included within the Bioconductor software suite (version 2.11) (50) and an Entrez Gene-specific probe set mapping (version 17.0.0) from the Molecular and Behavioral Neuroscience Institute (Brainarray) at the University of Michigan (51) (http://brainarray.mbni.med.umich.edu/Brainarray/Database/CustomCDF). Array quality was assessed by computing relative log expression (RLE) and normalized unscaled standard error (NUSE) using the affyPLM Bioconductor package (version 1.34.0) (52). Principal component analysis (PCA) was performed using the prcomp R function with expression values that had been normalized across all samples to a mean of zero and a standard deviation of one. Review of the PCA revealed an effect of the date the experiment was performed and the sex of the animal. However, since only 22% of the experimental variance was due to this effect, correction for batch effect was not performed. Pairwise differential expression was assessed using the moderated (empirical Bayesian) *t* test implemented in the limma package (version 3.14.4) (i.e., creating simple linear models with lmFit, followed by empirical Bayesian adjustment with eBayes). Correction for multiple comparisons was accomplished using the Benjamini-Hochberg false discovery rate (FDR) (53). All statistical analyses were performed using the R environment for statistical computing (version 2.15.1).

IPA. Ingenuity Pathway Analysis (IPA; version 01-16; Qiagen, Hilden, Germany) (14) was used to identify canonical pathways and upstream regulators predicted by differentially expressed genes (DEG) in our microarray data set. A data set containing gene identifiers, fold change, and FDR-corrected *P* values (*q* values) was uploaded, and a *q* value of <0.1 was set to identify molecules whose expression was significantly changed between treatment groups. Canonical pathway analysis identified the pathways from the IPA library that were significant to the data set, as determined using a right-tailed Fisher's exact test to calculate a *P* value and Benjamini-Hochberg multiple testing correction (53). Upstream regulator analysis was used to determine upstream regulators potentially affected by OSM neutralization. Changes in DEG were compared with effects derived in the literature complied in the Ingenuity Knowledge Base, comparing the direction of change to expectations from the literature. Significance was calculated using a right/tailed Fisher's exact test *P* value calculation. For both canonical pathway and upstream regulator analysis, z-scores were calculated based on the consistency of the pattern match of up- and downregulated genes in the data set and the expected activation and inhibition pattern downstream of a given regulator.

GSEA. Gene Set Enrichment Analysis (GSEA) (version 2.0.13) (16) was used to identify biological terms, pathways, and processes that were coordinately up- or downregulated with respect to anti-OSM treatment. The Entrez Gene identifiers of the human homologs of the genes interrogated by the array were ranked according to the moderated *t* statistic computed for the anti-OSM versus control IgG comparison. Mouse genes without a human homolog were removed, and the *t* statistics for multiple mouse genes with the same human homolog were averaged prior to ranking. This ranked list was then used to perform a preranked GSEA (default parameters with random seed 1234) using the Entrez Gene versions of the Biocarta, KEGG, Reactome, Gene Ontology (GO), and transcription factor and microRNA motif gene sets obtained from the Molecular Signatures Database (MSigDB), version 4.0 (17).

Tissue collection. Mice were euthanized at the time indicated in the text and figure legends. For bronchoalveolar lavage (BAL), the heart-lung block was surgically harvested, suspended by the trachea attached to a blunt catheter, and serially lavaged with 1 ml ice-cold PBS for a total volume of 10 ml. The first 1 ml BALF had cells removed by centrifugation (300 relative centrifugal force [RCF], 5 min) and fluid frozen at −80°C for total protein and cytokine assays. Cells from all washes were combined after centrifugation and used for total and differential cell counts. Cells were then frozen for RNA analysis. Left lungs postlavage were snap-frozen in liquid nitrogen and stored at –80°C for future RNA or protein analysis.

RNA isolation and qRT-PCR. For whole-lobe RNA, frozen tissue was homogenized in RLT buffer (Qiagen) using a Bullet Blender (Next Advance, Troy, NY) per the manufacturer's instructions, and RNA was isolated from homogenates using the RNeasy minikit (Qiagen) by following the manufacturer's protocol. For sorted cells, RNA was isolated using the RNeasy micro kit (Qiagen) by following the manufacturer's protocol. RNA concentrations were determined using a NanoDrop spectrophotometer (Thermo Scientific, Waltham, MA). Specific RNA transcripts were quantified using a TaqMan RNA-to-C_T 1-step kit and the QuantStudio 3 real-time PCR system (Thermo Scientific). All threshold cycle (C_T) values were normalized to 18S rRNA. Expression values are presented as fold inductions after normalization. Primers and probes for specific gene targets are listed in Table S1 in the supplemental material.

Immunoblotting. Total protein was extracted from frozen left lungs as previously described (12), with tissues homogenized in a Bullet Blender (Next Advance) according to the manufacturer's instructions. Total protein concentrations were determined using a bicinchoninic acid assay as described by the manufacturer (Millipore Sigma). Immunoblotting was performed using a NuPAGE 4 to 12% Bis-Tris gel (Thermo Fisher) and transferred onto nitrocellulose membranes (LI-COR, Lincoln, NE) via an X-Cell Blot II system (Thermo Fisher). Total protein per lane was visualized using Revert 700 total protein stain (LI-COR) according to the manufacturer's protocol and visualized using an Odyssey CLx imaging system (LI-COR). After destaining, membranes were blocked and incubated with primary and then secondary antibody (diluted to working concentrations as indicated in Table S2) and visualized by the Odyssey CLx imaging system. Digital images were annotated using Image Studio Lite (LI-COR) and quantified using Empiria Studio software (LI-COR). The normalized target signal for each sample was calculated for each lane based on densitometry of target signal per total protein. Fold change was calculated for each target by comparing the normalized signal for each sample to the average normalized signal of the control samples (either PBS or IgG control). Finally, for each transcription factor, the ratio of phosphoprotein to total protein was calculated. Significance was determined using Student's *t* test. All original immunoblots are depicted in Fig. S1 and S2 in the supplemental material.

Lung digest, single-cell suspension, and flow cytometry. Single-cell suspensions were generated from involved left lung lobes as previously described (40). Fluorescence-activated cell sorting (FACS) was performed on a FACSAria II (BD Biosciences, Franklin Lakes, NJ). For whole-lung digests, single-cell suspensions were sorted into epithelial cells (7AAD$^-$/CD45$^-$/EpCam$^+$), neutrophils (7AAD$^-$/CD45$^+$/EpCam$^-$/Ly6G$^+$/F4-80$^-$), macrophages (7AAD$^-$/CD45$^-$/EpCam$^+$/Ly6G$^-$/F4-80$^+$), and "other" leukocytes (7AAD$^-$/CD45$^+$/EpCam$^-$/Ly6G$^-$/F4-80$^-$). For BALF, resuspended cells were sorted into neutrophils (7AAD$^-$/CD45$^+$/Ly6G$^+$/F4-80$^-$) and macrophages (7AAD$^-$/CD45$^+$/Ly6G$^-$/F4-80$^+$). Peripheral blood was collected in a heparinized syringe from the inferior vena cava. Red blood cells were lysed with FACS lysing buffer (BD Biosciences) before neutrophils (7AAD$^-$/CD45$^+$/CD11b$^+$/Ly6G$^+$) and monocytes (7AAD$^-$/CD45$^+$/CD11b$^+$/CD115$^+$) were isolated. Example flow plots depicting this strategy are in Fig. S3. Flow cytometry antibodies are listed in Table S3. Cells from lung digests were sorted into PBS with 1% bovine serum albumin (BSA), centrifuged for 5 min at 300 RCF, resuspended in RNAprotect (Qiagen), and stored at −20°C for RNA isolation. Cells from BALF, peripheral blood, and epithelial subsets were sorted directly into RNAprotect (Qiagen) and stored.

Cell counts and differential. Cells from BALF were pooled, and total BAL cells were counted on a Luna FL fluorescence cell counter (Logos Biosystems, Annandale, VA) according to the manufacturer's instructions. For differential cell counts, approximately 1×10^5 cells in 100 μl were loaded onto cytocentrifuge funnels and cytocentrifuged onto microscopes slides at 800 $\times$ *g* for 3 min (Cytospin 4; Thermo Scientific). Slides were then stained with a Camco Stain Pak (Thermo Fisher). The percentages of neutrophils and macrophages were determined by visual inspection of a minimum of 100 cells per sample and used to calculate total neutrophil and macrophage counts in BALF.

Immunofluorescence. Mouse lungs were inflated by i.t. instillation of OCT compound (Thermo Fisher) followed by embedding and flash freezing in OCT. Lung blocks were then cut into 8-μm thin sections and stained with the primary antibodies anti-mouse F4/80, anti-mouse Ly6G, and anti-mouse OSM, followed by staining with Alexa 488 donkey anti-goat secondary antibody (1:1,000) and Alexa 594 donkey anti-rat secondary antibody (1:1,000), both from Jackson Immunoresearch. Details of antibodies used are in Table S3. Slides were imaged with a Leica DM4 microscope and Leica DFC 7000T camera and were acquired with Leica LAS X software. Images were captured using a 40$\times$ objective. All images were processed in FIJI using identical look-up table settings for all images of the same magnification.

***In vivo* depletion of alveolar macrophages.** Alveolar macrophages were depleted using clodronate liposomes as previously described (31). Briefly, 3 days prior to the planned *E. coli* infection, mice were intratracheally instilled with 50 μl vehicle containing 0.25 mg of either clodronate liposomes or control PBS liposomes (Liposoma, Amsterdam, The Netherlands; www.clodronateliposomes.com). Mice were euthanized for baseline cell counts or infected with *E. coli* for 6 or 24 h. BALF was collected for cell count determination, and left lobes were snap-frozen for RNA analysis.

ELISA. OSM cytokine levels were measured in BALF using an OSM DuoSet enzyme-linked immunosorbent assay (ELISA; R&D Systems, Minneapolis, MN) by following the manufacturer's instruction. Plates were read using a Synergy LX plate reader (BioTek, Winooski, VT).

Statistical analysis. For experiments not involving microarray data, statistical analysis was performed using GraphPad Prism (version 9; GraphPad, La Jolla, CA). Data are presented as a scatterplot with a bar representing the means and error bars denoting SEM. For all experiments, equivalence of variance was checked with an F test. Data with a significantly different variance were analyzed using a nonparametric test when possible or log transformed prior to statistical analysis. Statistical significance was defined as a *P* value of <0.05. Additional details regarding specific tests used and sample sizes are in the relevant figure legend.

Data availability. All data were submitted archived in the Gene Expression Omnibus (GEO series ID GSE155283).

SUPPLEMENTAL MATERIAL

Supplemental material is available online only.

SUPPLEMENTAL FILE 1, PDF file, 1.9 MB.

SUPPLEMENTAL FILE 2, PDF file, 2.9 MB.

SUPPLEMENTAL FILE 3, PDF file, 0.5 MB.

SUPPLEMENTAL FILE 4, PDF file, 0.05 MB.

ACKNOWLEDGMENTS

We thank the BU Flow Core, specifically Patrick Autissier, for assistance with flow cytometry sorting experiments and the BU Microarray and Sequencing Resource, specifically Adam Gower and Yuriy Alekseyev, for assistance with microarray assay and data analysis.

We received the following grants: National Heart, Lung, and Blood Institute (NHLBI) awards T32 HL007035 (K.E.T.), F32 HL120551 (K.E.T.), K08 HL130582 (K.E.T.), R01 HL111449 (L.J.Q.), and R35 HL-135756 (J.P.M.), National Institute of General Medical Sciences (NIGMS) award R01 GM120060 (L.J.Q.), and National Center for Advancing Translational Sciences (NCATS) award through the BU-CTSI, KL2 TR001411 (K.E.T.). Microarray analysis was supported by the microarray core, funded by NCATS award U54-TR001012.

REFERENCES

1. Murphy SL, Xu J, Kochanek KD, Arias E. 2018. Mortality in the United States, 2017. NCHS Data Brief 328:1–8.
2. GBD 2015 LRI Collaborators. 2017. Estimates of the global, regional, and national morbidity, mortality, and aetiologies of lower respiratory tract infections in 195 countries: a systematic analysis for the Global Burden of Disease Study 2015. Lancet Infect Dis 17:1133–1161. https://doi.org/10.1016/S1473-3099(17)30396-1.
3. Jain S, Self WH, Wunderink RG, Fakhran S, Balk R, Bramley AM, Reed C, Grijalva CG, Anderson EJ, Courtney DM, Chappell JD, Qi C, Hart EM, Carroll F, Trabue C, Donnelly HK, Williams DJ, Zhu Y, Arnold SR, Ampofo K, Waterer GW, Levine M, Lindstrom S, Winchell JM, Katz JM, Erdman D, Schneider E, Hicks LA, McCullers JA, Pavia AT, Edwards KM, Finelli L, Team CES, CDC EPIC Study Team. 2015. Community-acquired pneumonia requiring hospitalization among U.S. adults. N Engl J Med 373:415–427. https://doi.org/10.1056/NEJMoa1500245.
4. Quinton LJ, Walkey AJ, Mizgerd JP. 2018. Integrative physiology of pneumonia. Physiol Rev 98:1417–1464. https://doi.org/10.1152/physrev.00032.2017.
5. Guillet C, Fourcin M, Chevalier S, Pouplard A, Gascan H. 1995. ELISA detection of circulating levels of LIF, OSM, and CNTF in septic shock. Ann N Y Acad Sci 762:407–409. https://doi.org/10.1111/j.1749-6632.1995.tb32349.x.
6. Johnson SB, Lissauer M, Bochicchio GV, Moore R, Cross AS, Scalea TM. 2007. Gene expression profiles differentiate between sterile SIRS and early sepsis. Ann Surg 245:611–621. https://doi.org/10.1097/01.sla.0000251619.10648.32.
7. Gong Y, Yan X, Sun X, Chen T, Liu Y, Cao J. 2020. Oncostatin-M is a prognostic biomarker and inflammatory mediator for sepsis. J Infect Dis 221:1989–1998. https://doi.org/10.1093/infdis/jiaa009.
8. Grenier A, Combaux D, Chastre J, Gougerot-Pocidalo MA, Gibert C, Dehoux M, Chollet-Martin S. 2001. Oncostatin M production by blood and alveolar neutrophils during acute lung injury. Lab Investig 81:133–141. https://doi.org/10.1038/labinvest.3780220.
9. Kang HJ, Kang JS, Lee SH, Hwang SJ, Chae SW, Woo JS, Lee HM. 2005. Upregulation of oncostatin m in allergic rhinitis. Laryngoscope 115:2213–2216. https://doi.org/10.1097/01.mlg.0000187819.89889.4a.
10. West NR, Hegazy AN, Owens BMJ, Bullers SJ, Linggi B, Buonocore S, Coccia M, Gortz D, This S, Stockenhuber K, Pott J, Friedrich M, Ryzhakov G, Baribaud F, Brodmerkel C, Cieluch C, Rahman N, Muller-Newen G, Owens RJ, Kuhl AA, Maloy KJ, Plevy SE, Oxford I, Keshav S, Travis SPL, Powrie F. 2017. Oncostatin M drives intestinal inflammation and predicts response to tumor necrosis factor-neutralizing therapy in patients with inflammatory bowel disease. Nat Med 23:579–589. https://doi.org/10.1055/s-0037-1604794.
11. Mozaffarian A, Brewer AW, Trueblood ES, Luzina IG, Todd NW, Atamas SP, Arnett HA. 2008. Mechanisms of oncostatin M-induced pulmonary inflammation and fibrosis. J Immunol 181:7243–7253. https://doi.org/10.4049/jimmunol.181.10.7243.
12. Quinton LJ, Jones MR, Robson BE, Simms BT, Whitsett JA, Mizgerd JP. 2008. Alveolar epithelial STAT3, IL-6 family cytokines, and host defense during Escherichia coli pneumonia. Am J Respir Cell Mol Biol 38:699–706. https://doi.org/10.1165/rcmb.2007-0365OC.
13. Traber KE, Hilliard KL, Allen E, Wasserman GA, Yamamoto K, Jones MR, Mizgerd JP, Quinton LJ. 2015. Induction of STAT3-dependent CXCL5 expression and neutrophil recruitment by oncostatin-M during pneumonia. Am J Respir Cell Mol Biol 53:479–488. https://doi.org/10.1165/rcmb.2014-0342OC.
14. Kramer A, Green J, Pollard J, Jr, Tugendreich S. 2014. Causal analysis approaches in Ingenuity Pathway Analysis. Bioinformatics 30:523–530. https://doi.org/10.1093/bioinformatics/btt703.
15. Dey G, Radhakrishnan A, Syed N, Thomas JK, Nadig A, Srikumar K, Mathur PP, Pandey A, Lin SK, Raju R, Prasad TS. 2013. Signaling network of oncostatin M pathway. J Cell Commun Signal 7:103–108. https://doi.org/10.1007/s12079-012-0186-y.
16. Subramanian A, Tamayo P, Mootha VK, Mukherjee S, Ebert BL, Gillette MA, Paulovich A, Pomeroy SL, Golub TR, Lander ES, Mesirov JP. 2005. Gene set enrichment analysis: a knowledge-based approach for interpreting genome-wide expression profiles. Proc Natl Acad Sci U S A 102:15545–15550. https://doi.org/10.1073/pnas.0506580102.
17. Subramanian A, Kuehn H, Gould J, Tamayo P, Mesirov JP. 2007. GSEA-P: a desktop application for gene set enrichment analysis. Bioinformatics 23:3251–3253. https://doi.org/10.1093/bioinformatics/btm369.
18. Larrea E, Aldabe R, Gonzalez I, Segura V, Sarobe P, Echeverria I, Prieto J. 2009. Oncostatin M enhances the antiviral effects of type I interferon and activates immunostimulatory functions in liver epithelial cells. J Virol 83:3298–3311. https://doi.org/10.1128/JVI.02167-08.
19. Natesh K, Bhosale D, Desai A, Chandrika G, Pujari R, Jagtap J, Chugh A,

Ranade D, Shastry P. 2015. Oncostatin-M differentially regulates mesenchymal and proneural signature genes in gliomas via STAT3 signaling. Neoplasia 17:225–237. https://doi.org/10.1016/j.neo.2015.01.001.
20. Son HJ, Lee SH, Lee SY, Kim EK, Yang EJ, Kim JK, Seo HB, Park SH, Cho ML. 2017. Oncostatin M suppresses activation of IL-17/Th17 via SOCS3 regulation in CD4+ T cells. J Immunol 198:1484–1491. https://doi.org/10.4049/jimmunol.1502314.
21. Takata F, Dohgu S, Matsumoto J, Machida T, Sakaguchi S, Kimura I, Yamauchi A, Kataoka Y. 2018. Oncostatin M-induced blood-brain barrier impairment is due to prolonged activation of STAT3 signaling in vitro. J Cell Biochem 119:9055–9063. https://doi.org/10.1002/jcb.27162.
22. Chattopadhyay S, Tracy E, Liang P, Robledo O, Rose-John S, Baumann H. 2007. Interleukin-31 and oncostatin-M mediate distinct signaling reactions and response patterns in lung epithelial cells. J Biol Chem 282:3014–3026. https://doi.org/10.1074/jbc.M609655200.
23. Smyth DC, Kerr C, Li Y, Tang D, Richards CD. 2008. Oncostatin M induction of eotaxin-1 expression requires the convergence of PI3'K and ERK1/2 MAPK signal transduction pathways. Cell Signal 20:1142–1150. https://doi.org/10.1016/j.cellsig.2008.02.001.
24. Kwofie K, Scott M, Rodrigues R, Guerette J, Radford K, Nair P, Richards CD. 2015. Regulation of IL-17A responses in human airway smooth muscle cells by oncostatin M. Respir Res 16:14. https://doi.org/10.1186/s12931-014-0164-4.
25. Beigel F, Friedrich M, Probst C, Sotlar K, Goke B, Diegelmann J, Brand S. 2014. Oncostatin M mediates STAT3-dependent intestinal epithelial restitution via increased cell proliferation, decreased apoptosis and upregulation of SERPIN family members. PLoS One 9:e93498. https://doi.org/10.1371/journal.pone.0093498.
26. Zhang M, Wang C, Hu J, Lin J, Zhao Z, Shen M, Gao H, Li N, Liu M, Zheng P, Qiu C, Gao E, Wang H, Sun D. 2015. Notch3/Akt signaling contributes to OSM-induced protection against cardiac ischemia/reperfusion injury. Apoptosis 20:1150–1163. https://doi.org/10.1007/s10495-015-1148-7.
27. Traber KE, Dimbo EL, Symer EM, Korkmaz FT, Jones MR, Mizgerd JP, Quinton LJ. 2019. Roles of interleukin-11 during acute bacterial pneumonia. PLoS One 14:e0221029. https://doi.org/10.1371/journal.pone.0221029.
28. Hurst SM, McLoughlin RM, Monslow J, Owens S, Morgan L, Fuller GM, Topley N, Jones SA. 2002. Secretion of oncostatin M by infiltrating neutrophils: regulation of IL-6 and chemokine expression in human mesothelial cells. J Immunol 169:5244–5251. https://doi.org/10.4049/jimmunol.169.9.5244.
29. Cross A, Edwards SW, Bucknall RC, Moots RJ. 2004. Secretion of oncostatin M by neutrophils in rheumatoid arthritis. Arthritis Rheum 50:1430–1436. https://doi.org/10.1002/art.20166.
30. Pothoven KL, Norton JE, Suh LA, Carter RG, Harris KE, Biyasheva A, Welch K, Shintani-Smith S, Conley DB, Liu MC, Kato A, Avila PC, Hamid Q, Grammer LC, III, Peters AT, Kern RC, Tan BK, Schleimer RP. 2016. Neutrophils are a major source of the epithelial barrier disrupting cytokine oncostatin M in patients with mucosal airways disease. J Allergy Clin Immunol 139:1966–1978. https://doi.org/10.1016/j.jaci.2016.10.039.
31. Traber KE, Symer EM, Allen E, Kim Y, Hilliard KL, Wasserman GA, Stewart CL, Jones MR, Mizgerd JP, Quinton LJ. 2017. Myeloid-epithelial cross talk coordinates synthesis of the tissue-protective cytokine leukemia inhibitory factor during pneumonia. Am J Physiol Lung Cell Mol Physiol 313:L548–L558. https://doi.org/10.1152/ajplung.00482.2016.
32. Young PY, Mueller TF, Sis B, Churchill TA, Khadaroo RG. 2020. Oncostatin M plays a critical role in survival after acute intestinal ischemia: reperfusion injury. Surg Infect 21:799–806. https://doi.org/10.1089/sur.2019.193.
33. Nagahama KY, Togo S, Holz O, Magnussen H, Liu X, Seyama K, Takahashi K, Rennard SI. 2013. Oncostatin M modulates fibroblast function via STAT3. Am J Respir Cell Mol Biol 49:582–591. https://doi.org/10.1165/rcmb.2012-0460OC.
34. Wong S, Botelho FM, Rodrigues RM, Richards CD. 2014. Oncostatin M overexpression induces matrix deposition, STAT3 activation, and SMAD1 dysregulation in lungs of fibrosis-resistant BALB/c mice. Lab Investig 94:1003–1016. https://doi.org/10.1038/labinvest.2014.81.
35. Quinton LJ, Mizgerd JP. 2015. Dynamics of lung defense in pneumonia: resistance, resilience, and remodeling. Annu Rev Physiol 77:407–430. https://doi.org/10.1146/annurev-physiol-021014-071937.
36. Luzina IG, Atamas SP, Wise R, Wigley FM, Choi J, Xiao HQ, White B. 2003. Occurrence of an activated, profibrotic pattern of gene expression in lung CD8+ T cells from scleroderma patients. Arthritis Rheum 48:2262–2274. https://doi.org/10.1002/art.11080.
37. Kastl SP, Speidl WS, Katsaros KM, Kaun C, Rega G, Assadian A, Hagmueller GW, Hoeth M, de Martin R, Ma Y, Maurer G, Huber K, Wojta J. 2009. Thrombin induces the expression of oncostatin M via AP-1 activation in human macrophages: a link between coagulation and inflammation. Blood 114:2812–2818. https://doi.org/10.1182/blood-2009-01-200915.
38. Albasanz-Puig A, Murray J, Preusch M, Coan D, Namekata M, Patel Y, Dong ZM, Rosenfeld ME, Wijelath ES. 2011. Oncostatin M is expressed in atherosclerotic lesions: a role for Oncostatin M in the pathogenesis of atherosclerosis. Atherosclerosis 216:292–298. https://doi.org/10.1016/j.atherosclerosis.2011.02.003.
39. Leach HG, Chrobak I, Han R, Trojanowska M. 2013. Endothelial cells recruit macrophages and contribute to a fibrotic milieu in bleomycin lung injury. Am J Respir Cell Mol Biol 49:1093–1101. https://doi.org/10.1165/rcmb.2013-0152OC.
40. Yamamoto K, Ahyi AN, Pepper-Cunningham ZA, Ferrari JD, Wilson AA, Jones MR, Quinton LJ, Mizgerd JP. 2014. Roles of lung epithelium in neutrophil recruitment during pneumococcal pneumonia. Am J Respir Cell Mol Biol 50:253–262. https://doi.org/10.1165/rcmb.2013-0114OC.
41. Setiadi H, Yago T, Liu Z, McEver RP. 2019. Endothelial signaling by neutrophil-released oncostatin M enhances P-selectin-dependent inflammation and thrombosis. Blood Adv 3:168–183. https://doi.org/10.1182/bloodadvances.2018026294.
42. Doerschuk CM. 2001. Mechanisms of leukocyte sequestration in inflamed lungs. Microcirculation 8:71–88. https://doi.org/10.1111/j.1549-8719.2001.tb00159.x.
43. Kalil AC, Metersky ML, Klompas M, Muscedere J, Sweeney DA, Palmer LB, Napolitano LM, O'Grady NP, Bartlett JG, Carratala J, El Solh AA, Ewig S, Fey PD, File TM, Jr, Restrepo MI, Roberts JA, Waterer GW, Cruse P, Knight SL, Brozek JL. 2016. Management of adults with hospital-acquired and ventilator-associated pneumonia: 2016 clinical practice guidelines by the Infectious Diseases Society of America and the American Thoracic Society. Clin Infect Dis 63:e61–e111. https://doi.org/10.1093/cid/ciw353.
44. Jones BE, Herman DD, Dela Cruz CS, Waterer GW, Metlay JP, Ruminjo JK, Thomson CC. 2020. Summary for clinicians: clinical practice guideline for the diagnosis and treatment of community-acquired pneumonia. Ann Am Thorac Soc 17:133–138. https://doi.org/10.1513/AnnalsATS.201909-704CME.
45. Peleg AY, Hooper DC. 2010. Hospital-acquired infections due to gram-negative bacteria. N Engl J Med 362:1804–1813. https://doi.org/10.1056/NEJMra0904124.
46. Quinton LJ, Blahna MT, Jones MR, Allen E, Ferrari JD, Hilliard KL, Zhang X, Sabharwal V, Algul H, Akira S, Schmid RM, Pelton SI, Spira A, Mizgerd JP. 2012. Hepatocyte-specific mutation of both NF-kappaB RelA and STAT3 abrogates the acute phase response in mice. J Clin Investig 122:1758–1763. https://doi.org/10.1172/JCI59408.
47. Quinton LJ, Jones MR, Robson BE, Mizgerd JP. 2009. Mechanisms of the hepatic acute-phase response during bacterial pneumonia. Infect Immun 77:2417–2426. https://doi.org/10.1128/IAI.01300-08.
48. Irizarry RA, Hobbs B, Collin F, Beazer-Barclay YD, Antonellis KJ, Scherf U, Speed TP. 2003. Exploration, normalization, and summaries of high density oligonucleotide array probe level data. Biostatistics 4:249–264. https://doi.org/10.1093/biostatistics/4.2.249.
49. Gautier L, Cope L, Bolstad BM, Irizarry RA. 2004. affy–analysis of Affymetrix GeneChip data at the probe level. Bioinformatics 20:307–315. https://doi.org/10.1093/bioinformatics/btg405.
50. Gentleman RC, Carey VJ, Bates DM, Bolstad B, Dettling M, Dudoit S, Ellis B, Gautier L, Ge Y, Gentry J, Hornik K, Hothorn T, Huber W, Iacus S, Irizarry R, Leisch F, Li C, Maechler M, Rossini AJ, Sawitzki G, Smith C, Smyth G, Tierney L, Yang JY, Zhang J. 2004. Bioconductor: open software development for computational biology and bioinformatics. Genome Biol 5:R80. https://doi.org/10.1186/gb-2004-5-10-r80.
51. Dai M, Wang P, Boyd AD, Kostov G, Athey B, Jones EG, Bunney WE, Myers RM, Speed TP, Akil H, Watson SJ, Meng F. 2005. Evolving gene/transcript definitions significantly alter the interpretation of GeneChip data. Nucleic Acids Res 33:e175. https://doi.org/10.1093/nar/gni179.
52. Brettschneider J, Collin F, Bolstad BM, Speed TP. 2008. Quality assessment for short oligonucleotide microarray data. Technometrics 50:241–264. https://doi.org/10.1198/004017008000000334.
53. Benjamini Y, Hochberg Y. 1995. Controlling the false discovery rate: a practical and powerful approach to multiple testing. J R Stat Soc Series B Stat Methodol 57:289–300. https://doi.org/10.1111/j.2517-6161.1995.tb02031.x.